Materials Chemistry and Physics 326 (2024) 129787

Contents lists available at ScienceDirect

Materials Chemistry and Physics

journal homepage: www.elsevier.com/locate/matchemphys

Polymer-like hydrogenated amorphous carbon thin films fabricated by plasma-enhanced chemical vapor deposition of cyclohexane precursor

Thomas Poche, Rajib Chowdhury, Seonhee Jang *

Department of Mechanical Engineering, University of Louisiana at Lafayette, Lafayette, LA, 70503, USA

HIGHLIGHTS

- Hydrogenated amorphous carbon films were fabricated by chemical vapor deposition.
- A cyclohexane precursor was adopted for deposition of amorphous carbon films.
- Chemical structure of amorphous carbon films depended on deposition parameters.
- Amorphous carbon films were transparent and hydrophobic.
- Amorphous carbon films had a wide optical bandgap range of 3.08–3.69 eV.

GRAPHICAL ABSTRACT

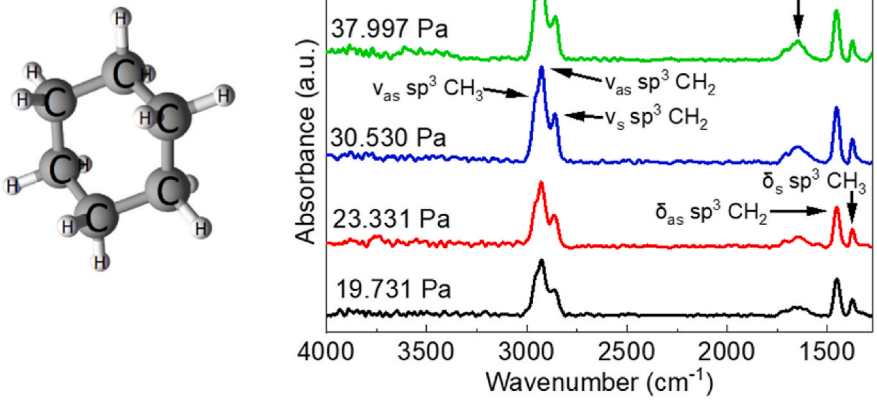

ARTICLE INFO

Keywords:
Hydrogenated amorphous carbon
Plasma-enhanced chemical vapor deposition
Cyclohexane
Optical bandgap
Refractive index

ABSTRACT

Hydrogenated amorphous carbon (a-C:H) films were fabricated by plasma-enhanced chemical vapor deposition (PECVD) of a cyclohexane precursor at ambient temperature at varying deposition pressures from 19.73 to 38.00 Pa and varying plasma powers from 20 to 80 W. The deposition rate of the a-C:H films was strongly dependent on the deposition conditions. The films were all optically transparent with extinction coefficient below 0.0042. The refractive index as an indicator of the film's density varied depending on the deposition conditions. Their surfaces were all hydrophobic regardless of the deposition conditions. The a-C:H films had wide optical bandgaps ranging from 3.09 to 3.69 eV. The refractive index and FTIR spectra were consistent with those of polymer-like a-C:H films. As the deposition pressure decreased and plasma power increased, the intensity of a dominant peak of CH_x stretching mode in the FTIR spectra decreased. The relative hydrogen content of the a-C:H films was estimated from an FTIR analysis and determined to have an inverse relationship with refractive index. These results indicated that the formation of more energetic plasmas during deposition at lower pressures and higher plasma powers led to the a-C:H films with reduced hydrogen content and increased density. The observed film properties

* Corresponding author.
E-mail address: seonhee.jang@louisiana.edu (S. Jang).

https://doi.org/10.1016/j.matchemphys.2024.129787
Received 29 September 2023; Received in revised form 9 July 2024; Accepted 29 July 2024
Available online 30 July 2024

could be advantageous for several applications, particularly as protective, wear-resistant, low-friction, or anti-reflective coatings for optical windows.

1. Introduction

Hydrogenated amorphous carbon (a-C:H) films have garnered significant attention due to their wide range of desirable properties, which are highly dependent on their hydrogen (H) content and the hybridization of their carbon (C) atoms as sp^3, sp^2, or sp bonded [1–4]. In C-C sp^3 hybridization, the valence electrons of the carbon atom form four strong σ bonds with its neighboring atoms in a tetrahedral configuration. The strong σ bonds cause a-C:H materials with significant C-C sp^3 hybridization to have high density, hardness, chemical inertness, and electrical resistivity [5–10]. These films are referred to as diamond-like a-C:H and have been applied as protective coatings for tools and cutting instruments due to their superior mechanical properties [11–14]. The chemical inertness of these films expands their application into use as biocompatible coatings and hard masks in semiconductor processing [7]. Additionally, the low conductivity and dielectric constant of these films has led them to be considered for use in integrated circuit chips as inter-metal dielectric materials [13,15]. The utilization of high-density plasma can result in the formation of tetrahedral a-C:H films, a sub-set of diamond-like a-C:H films which have an even higher concentration of C-C sp^3 hybridization (~80 %) [5,11,16]. In C-C sp^2 hybridization, the valence electrons of the carbon atom form three σ bonds and one π bond [17]. The delocalized electron in the π bond causes increased chemical sensitivity, increased electrical conductivity, and a reduced optical bandgap in a-C:H films with significant C-C sp^2 bonding, sometimes referred to as graphite-like a-C:H films [3,16,18–21]. The optical band gap and electrical conductivity of the a-C:H films can be altered significantly by controlling the C-C sp^2/sp^3 ratio, and the films have been considered for application as amorphous semiconductor materials [22,23]. In C-C sp hybridization, the valence electrons of the carbon atom form two σ bonds and two π bonds. As C-C sp hybridization can only create olefinic chains, it is not typically present within a-C:H films in significant amounts. Polymer-like a-C:H films, which are the focus of this study, have a high H content (40–50 %) and primarily consist of C-H sp^3 bond sites [5]. The significant amount of H passivates dangling bonds, preventing cross-linking and causing polymer-like a-C:H films to have a comparatively low density and soft matrix [16,24,25]. The friction coefficient of a-C:H films is also affected by the H content, which enhances the formation of a lubricating transfer layer on the surface of the material [26]. Polymer-like a-C:H films do not exhibit the same suite of desirable properties as the other a-C:H sub-classifications and have received little attention.

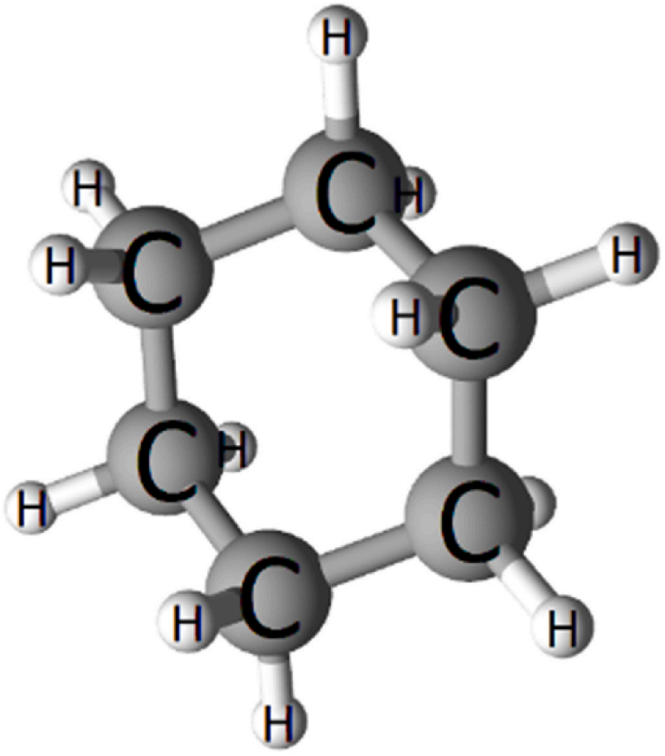

Fig. 1. Molecular structure of the cyclohexane precursor.

The most popular method of producing a-C:H films is using plasma-enhanced chemical vapor deposition (PECVD) [9,22]. Selecting the deposition parameters of PECVD is vital for controlling the characteristics of the a-C:H film, as factors such as deposition pressure, plasma power, gas flow rate, and temperature all have a significant impact on the properties of the film [16,25,27]. In this study, polymer-like a-C:H films were prepared by PECVD of a cyclohexane (C_6H_{12}) precursor at ambient temperature. The cyclohexane precursor was chosen for a-C:H film deposition for this study because it allows for increased deposition rates to be achieved at relatively low temperatures and bias voltages compared to other common carbon sources. The effect of varying deposition pressure and plasma power on material properties of the a-C:H films was determined. Optical and physical properties including refractive index, extinction coefficient, optical bandgap, contact angle, and surface roughness were analyzed. Additionally, the chemical structure of the a-C:H films was examined, and a hydrogen content estimation was performed.

2. Experimental details

The a-C:H thin films were deposited by plasma-enhanced chemical vapor deposition (PECVD) of a cyclohexane (C_6H_{12}, Sigma Aldrich, 99.5 % purity) precursor. Fig. 1 shows the molecular structure of the cyclohexane precursor. The six central carbon (C) atoms are connected through single bonds to form an aromatic ring, and all of the C atoms have single bonds to two outer hydrogen (H) atoms. Cyclohexane is relatively safer and more economical than any common carbon sources. Cyclohexane has a lower bond dissociation energy (282.4 kJ/mol) than other carbon liquid precursors such as methane (CH_4, 431 kJ/mol) and benzene (C_6H_6, 410 kJ/mol), and a relatively low ionization potential of ~9.75 eV [5,28]. In the PECVD process, this allows cyclohexane precursor to achieve high deposition rates at relatively low bias voltages and temperatures, which is advantageous for the study of polymer-like a-C:H films compared to any other carbon precursors [5].

Phosphorous-doped n-type Si (100) wafers with four-inch diameter purchased from MSE Supplies were utilized for the deposition process. The substrates had an average thickness of 525 μm and a resistivity of 1–10 Ω cm. For each deposition, two identical Si substrates were utilized, each shaped like a quarter circle with a radius of 5 cm. The substrates were cleaned through 5 min of ultrasonic cleaning in acetone, followed by an additional 5 min of ultrasonic cleaning in ethanol. The substrates were then rinsed three times using deionized water. Any excess moisture on the surface of the substrate was removed by a nitrogen blow gun before loading in the PECVD reactor. The PECVD system utilized for deposition of the a-C:H films had a radio frequency (RF) plasma generator at 13.56 MHz. Prior to the deposition process, the substrates were loaded onto a susceptor, which was maintained at a distance of 20 mm from the showerhead. The chamber pressure was then reduced to approximately 0.5 Pa using a dry screw pump. Argon (Ar) plasma cleaning was then conducted. For this purpose, Ar with a purity

Table 1
Two sets of deposition conditions of a-C:H films at varying deposition pressures and plasma powers, respectively.

Deposition conditions of set 1		Deposition conditions of set 2	
Deposition pressure (Pa)	Plasma power (W)	Deposition pressure (Pa)	Plasma power (W)
19.73	80	20.27	20
23.33	80	19.73	40
30.53	80	20.93	60
38.00	80	19.73	80

of 99.999 % was utilized. A mass flow controller (MFC) was used to maintain the flow of Ar at 50 sccm, and the chamber pressure reached 16.8 Pa. Then, the RF plasma power was turned on with 50 W and the plasma cleaning was conducted for 3 min. After the plasma cleaning, the chamber pressure was reduced to approximately 0.5 Pa, which was a base pressure before deposition. An Ar carrier gas maintained at a flow of 40 sccm using an MFC was passed through a bubbler system containing the cyclohexane precursor. Although the bubbler was maintained at ambient temperature, the gas lines between the bubbler and the chamber were heated to 40 °C to ensure a stable flow of the vaporized precursor and to prevent unwanted condensation. As the vaporized cyclohexane molecules and Ar carrier gas flowed from the bubbler to the reactor chamber, a pressure flow controller (PFC) varied the pressure flow values between 200 and 400 Torr. The chamber pressure during deposition was controlled by changing the PFC value.

Table 1 shows two sets of deposition conditions for the a-C:H films by varying deposition pressures and plasma powers. The effects of either deposition pressure or plasma power on the characteristics of the polymer-like a-C:H films were investigated. For the first set of the a-C:H films, an RF plasma power of 80 W supplied from the RF power generator was fixed, and the deposition pressure was varied from 19.73 to 38.00 Pa. For the second set of the a-C:H films, the pressure was maintained between 19.73 and 20.93 Pa and RF plasma powers supplied from the RF power generator were 20, 40, 60, and 80 W. For the second set, the deposition pressure was initially intended to be set as 20 Pa equally for all conditions. Although all the deposition conditions were the same except for the power, the deposition pressure could not be maintained at 20 Pa for all conditions due to system limitations. A maximum deviation of 0.93 Pa was obtained but this is acceptable to isolate the effect of varying plasma power on the a-C:H films. Deposition process was conducted for 5 min at ambient temperature of 18–20 °C for all the a-C:H films. The deposition condition at a pressure of 19.73 Pa and a plasma power of 80 W appears in both sets of varying pressures and varying plasma powers. It should be noted that the power was measured slightly lower (1–2 W below) than the set value when the plasma was generated during deposition process.

The samples after deposition were ready for various characterization techniques to be performed. Spectroscopic ellipsometry (alpha-SE, J.A. Woollam) with a 633 nm light source was used to measure the thickness, refractive index, and extinction coefficient of the a-C:H films. A range of 210–2500 nm was measured at angles of 50, 60, and 70°. A Cauchy model was used to fit the measured data. The refractive index and extinction coefficient values were taken at 633 nm. The deposition rate was calculated by dividing the thickness value found through ellipsometry by the deposition time. The thickness, refractive index, and extinction coefficient of the films were measured three times for each sample, with the averages reported in the results. Additionally, spectroscopic ellipsometry was used to estimate the optical band gap (E_g) of the a-C:H films. Spectroscopic ellipsometry data were collected three times for each sample and one of them was utilized to calculate the optical bandgap. To perform this estimation, the optical properties measured by spectroscopic ellipsometry were fitted using two Cody-Lorentz oscillators. The absorption coefficient (α) of the film was then calculated by $\alpha = \frac{4\pi k}{\lambda}$, where k is the extinction coefficient and λ is the wavelength of light in nm. Photon energy (E) in eV was calculated by $E = 1239.8/\lambda$. A "Tauc plot" was formed by plotting $(\alpha E)^{1/2}$ vs. E, which is commonly used to determine the optical bandgap of amorphous materials [29]. The linear region of the Tauc plot was extrapolated to the x-axis to determine E_g. Contact angle goniometry (L2004A, Oscilla) was performed three times for each film to determine the surface wettability of the a-C:H films. Atomic force microscopy (AFM, SmartSPM, Horiba) was used to determine the surface morphology and RMS (root mean square) roughness of the a-C:H films. The reported data for surface morphology and RMS roughness were based on a single measurement for each film due to limited time for the AFM utilization. Fourier transform infrared (FTIR) spectroscopy (Invenio-S, Bruker) was used to analyze the chemical composition of the a-C:H films, and to estimate their relative hydrogen content. The FTIR measurements were conducted three times for each film and one of them was used to calculate the relative hydrogen content. The FTIR instrument featured a Vari GATR attachment and scanned 64 times in the 4000-600 cm^{-1} wavenumber range at a resolution of 4 cm^{-1}. The relative hydrogen content (C) was estimated by $C = A\int\frac{\alpha}{\omega}d\omega$, over the range of the CH_x peak structure at 3100-2800 cm^{-1}, where α is the absorption coefficient, ω is wavenumber in cm^{-1}, and A is a constant scaling factor [30–32]. It should be noted that unbound, optically inactive hydrogen has been shown to be present within a-C:H films, which does not appear in the FTIR spectra [24,33]. This method of hydrogen content estimation assumes that the ratio between bound and unbound hydrogen atoms is

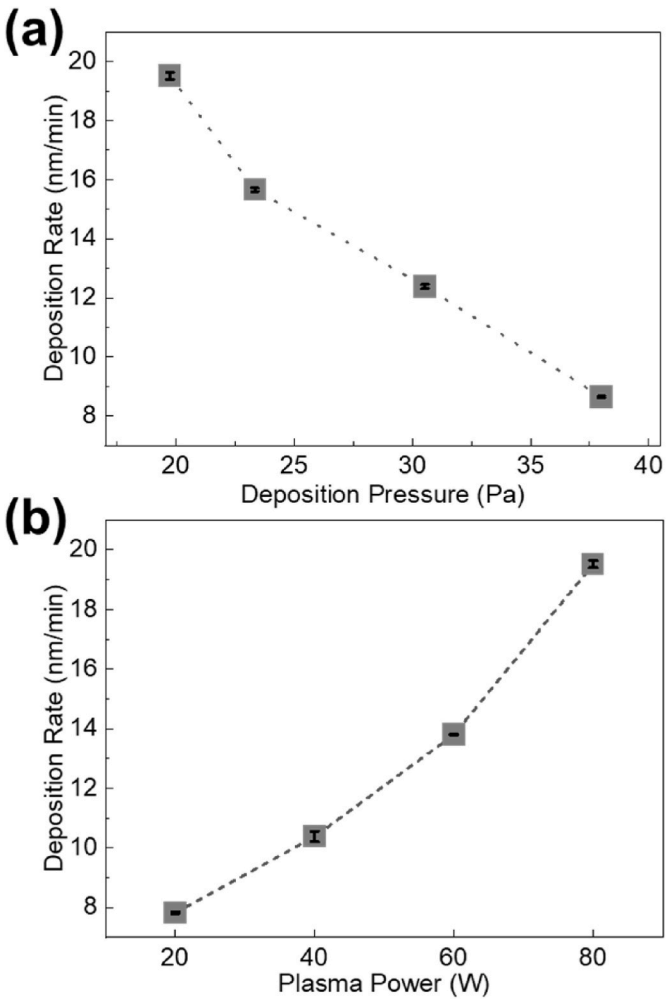

Fig. 2. Deposition rate of a-C:H films deposited at (a) varying deposition pressures between 19.73 and 38.00 Pa, and (b) varying plasma powers of 20, 40, 60, and 80 W.

Table 2
Optical and physical properties of a-C:H films deposited at varying deposition pressures and plasma powers.

Deposition conditions		Thickness (nm)	Refractive index	Extinction coefficient	Optical bandgap (eV)	Contact angle (degree)	RMS roughness (nm)
Deposition pressure (Pa)	19.73	97.58	1.547	0.0042	3.39	96.70	0.31
	23.33	78.29	1.544	0.0020	3.59	96.85	0.28
	30.53	61.92	1.541	0.0013	3.69	97.07	0.27
	38.00	43.21	1.530	0.0036	3.31	98.05	0.27
Plasma power (W)	20	39.12	1.539	0.0033	3.09	95.23	0.20
	40	51.89	1.540	0.0016	3.42	98.15	0.23
	60	69.01	1.544	0.0014	3.56	95.12	0.22
	80	97.58	1.547	0.0012	3.39	96.70	0.31

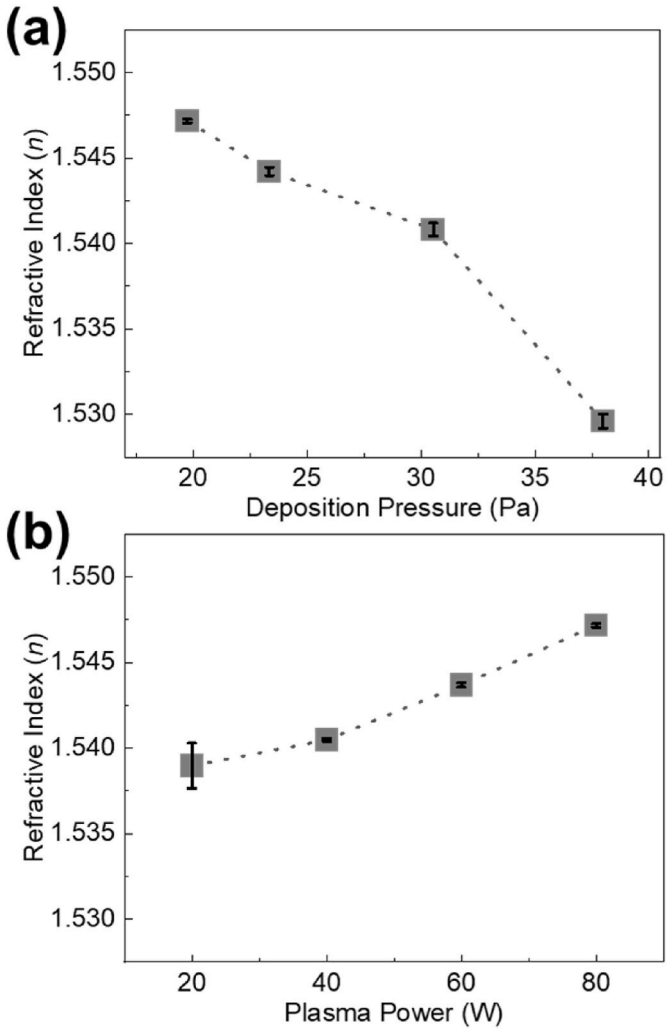

Fig. 3. Refractive index of a-C:H films deposited at (a) varying deposition pressures between 19.73 and 38.00 Pa, and (b) varying plasma powers of 20, 40, 60, and 80 W.

consistent within the a-C:H films so that a comparison can be made between them.

3. Results and discussion

3.1. Deposition rate

Fig. 2(a) and (b) shows the deposition rate of the a-C:H films deposited at varying deposition pressures and plasma powers, respectively. Changes in both the deposition pressure and the plasma power had a significant effect on the deposition rate of the a-C:H films. As the pressure increased from 19.73 to 38.00 Pa, the deposition rate decreased from 19.52 to 8.64 nm/min. Likewise, as the plasma power increased from 20 to 80 W, the deposition rate increased from 7.82 to 19.52 nm/min. In PECVD, the deposition rate is controlled by the relationship between the competing processes of polymerization and ablation [34]. Polymerization results in the deposition of precursor fragments onto the substrate surface, while ablation results in the removal of surface molecules through energetic plasma interactions. The more energetic plasma which was formed at lower deposition pressures and higher plasma powers more effectively dissociated the cyclohexane precursor into hydrocarbon fragments. This increased the concentration of hydrocarbon fragments in the plasma, resulting in a higher rate of polymerization. The increase of deposition rate at lower pressures and higher plasma powers indicates that polymerization was the dominant process in this case.

3.2. Optical and physical properties

Table 2 presents the optical and physical properties of a-C:H films deposited at varying deposition pressures and plasma powers. The optical properties reported included refractive index, extinction coefficient and optical bandgap, while the physical properties reported included contact angle and RMS roughness.

Fig. 3(a) and (b) shows the refractive index of the a-C:H films deposited at varying deposition pressures and plasma powers, respectively. These values can also be found in Table 2. As the deposition pressure increased from 19.73 to 38.00 Pa, the refractive index values decreased from 1.547 to 1.530. As the plasma power was increased from 20 to 80 W, the refractive index values increased slightly from 1.539 to 1.547. The range of refractive index values found (~1.540) is consistent with polymer-like a-C:H films [24]. For diamond-like a-C:H films, refractive index values up to ~2.1 are expected [24]. It is known that a higher refractive index is correlated with an increased film density [2,35]. Hydrogen atoms in the a-C:H film passivate dangling bonds and prevent cross-linking, so the film density would be greater for a-C:H films with reduced hydrogen content [24,25]. In this way, a higher refractive index can indicate that an a-C:H film has a reduced hydrogen content. This suggests that the films deposited at lower pressures and higher powers had an increased film density and reduced hydrogen content. At lower pressures and higher plasma powers, there was an increased likelihood for hydrogen to be removed from the film through additional ion bombardment from the more energetic plasma [26]. The carbon atoms then bonded together to form primarily sp^2 C-C bonding sites [26,36].

The sub-plantation model is widely accepted to describe the formation of C-C sp^3 sites in a-C:H films. It suggests that sp^3 sites are formed by the penetration of high energy carbon ions beneath the surface layer of the a-C:H film [7,37]. These sub-planted ions create structural disruption in the existing sp^2 C-C hybridized network, causing adjacent atoms to rearrange into sp^3 bonds [3,7]. It is possible that the more energetic plasma generated at lower pressures and greater plasma powers could cause an additional number of carbon ions to sub-plant within the films and form sp^3 C-C sites. However, the range of refractive index values

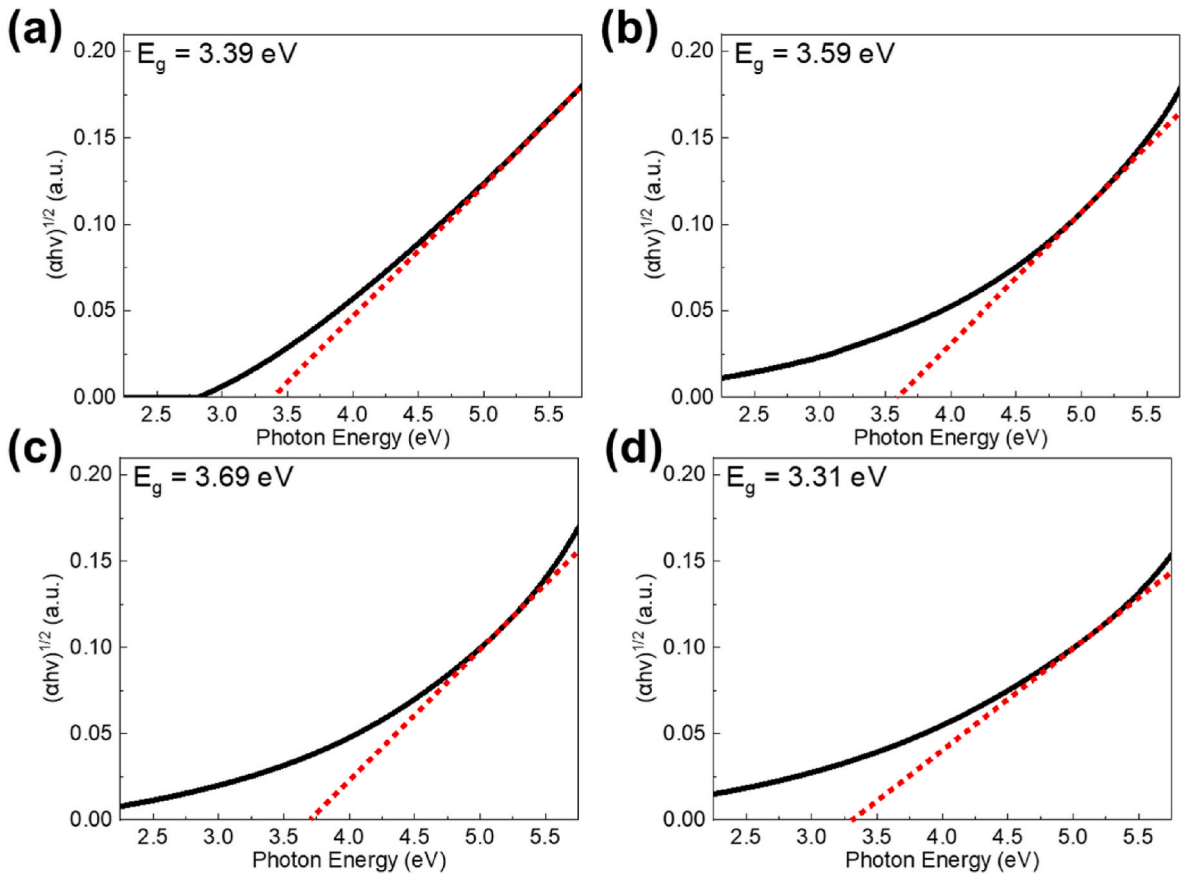

Fig. 4. Tauc plots of a-C:H films deposited at pressures of (a) 19.73, (b) 23.33, (c) 30.53, and (d) 38.00 Pa.

does not suggest that a significant amount of sp^3 C-C bonding was present within the film.

The extinction coefficient values of the a-C:H films when the deposition pressure and the plasma power were varied can be seen in Table 2. As both the deposition pressure and the plasma power were varied, the extinction coefficient values remained low, with a maximum value of 0.0042. Due to the low extinction coefficient, all the films can be considered optically transparent. For context, a-C:H films are often utilized as hardmask materials, which requires the material to have an extinction coefficient below 0.14 [7,38].

Fig. 4(a)–(d) present the Tauc plots of the a-C:H films deposited at varying deposition pressures of 19.73, 23.33, 30.53, and 38.00 Pa, respectively. The solid black line represents the Tauc curve, and the dashed red line represents the extrapolation of the linear region to the x-axis. The optical bandgap value (E_g) was estimated as the intercept point between the x-axis and the extrapolated linear region. The optical bandgap values are also reported in Table 2. The optical bandgap values for the a-C:H films ranged from 3.39 to 3.69 eV, which is within the expected range for polymer-like a-C:H films [5].

Fig. 5(a)–(d) show the Tauc plots of the a-C:H films deposited at varying plasma powers of 20, 40, 60, and 80 W, respectively. The optical bandgap values are also reported in Table 2. Again, the optical bandgap was determined by the intercept point between the x-axis and the extrapolated linear region. The optical bandgap of the films deposited at varying plasma powers ranged from 3.08 to 3.56 eV. The a-C:H films deposited at the lowest pressure of 19.73 Pa and the films deposited at plasma powers of 20 and 80 W had differently shaped Tauc curves compared to the other films. The sharp absorption edge of the Tauc curve suggests that these films had a direct optical bandgap, while the other samples had Tauc curves characteristic of an indirect optical bandgap [29]. The Tauc curve of many of the films displays the gradual decrease below the optical bandgap value known as an 'Urbach tail', caused by the amorphous arrangement of atoms within the a-C:H films [29].

The optical band gap is affected by the size of C-C sp^2 clusters and decreases as C-C sp^2 concentration increases [24,26,36]. This suggests that the films deposited at 19.73 and 38.00 Pa had an increased concentration of C-C sp^2 bonding compared to the films deposited at 23.33 and 30.53 Pa. It is also suggested that the film deposited at 20 W had an increased C-C sp^2 concentration compared to the other a-C:H films deposited at varying plasma powers, while the film deposited at 60 W had the lowest C-C sp^2 concentration. However, the optical bandgap of the a-C:H films must be estimated due to their amorphous nature, and assumptions about the microstructure based only on the optical bandgap estimation should be restricted.

The contact angles of the a-C:H films deposited at varying deposition pressures and plasma powers are also presented in Table 2. For context, a contact angle greater than 90° denotes that a material is hydrophobic in nature. All the a-C:H films were hydrophobic displaying their contact angles above 90°, and the contact angle increased slightly from 96.70 to 98.05° as the deposition pressure increased from 19.73 to 38.00 Pa. No clear trend was seen in the contact angle values as the plasma power was varied. The film deposited at 60 W had the smallest contact angle value of 95.12°, while the film at 40 W had the largest contact angle value of 98.15°.

Fig. 6(a)–(d) shows the surface morphology of the a-C:H films deposited at varying deposition pressures of 19.73, 23.33, 30.53, and 38.00 Pa, respectively. The surface morphology for each sample was measured over a 1 × 1 μm area. Vertical scale bars on the right side of each scan display the difference in height between the highest and lowest points in the scanned area. The RMS roughness value of the a-C:H films is displayed in the top right corner of each scan and in Table 2. As

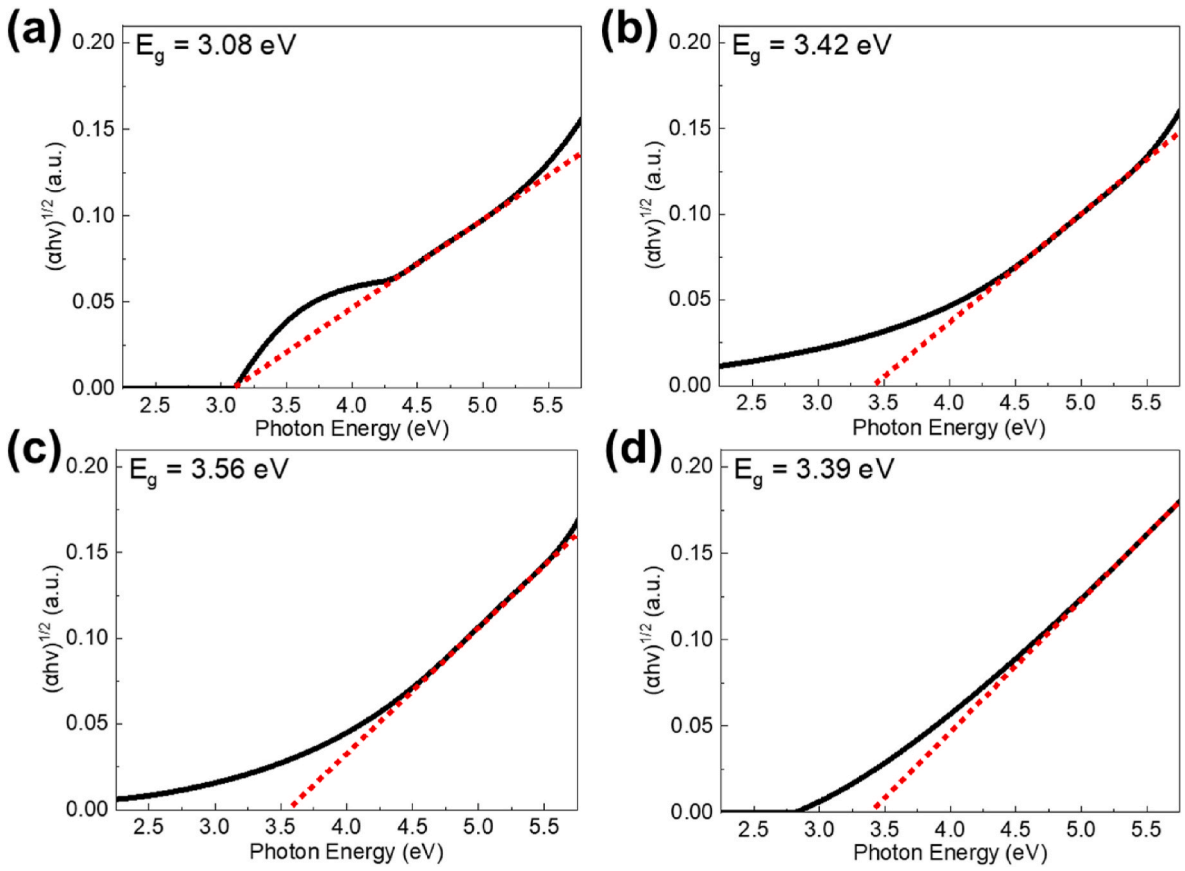

Fig. 5. Tauc plots of a-C:H films deposited at plasma powers of (a) 20, (b) 40, (c) 60, and (d) 80 W.

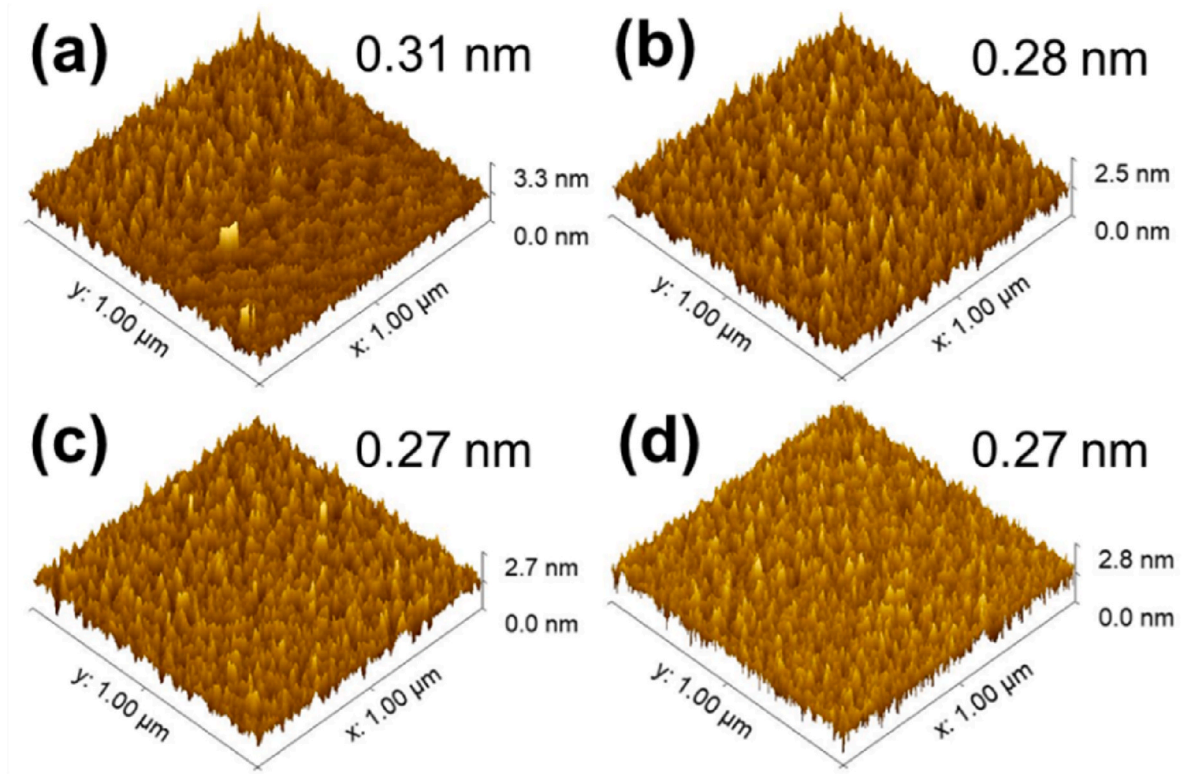

Fig. 6. AFM surface morphology of a-C:H films deposited at pressures of (a) 19.73, (b) 23.33, (c) 30.53, and (d) 38.00 Pa. The values in the top right corner of each image represent the RMS roughness value for each sample.

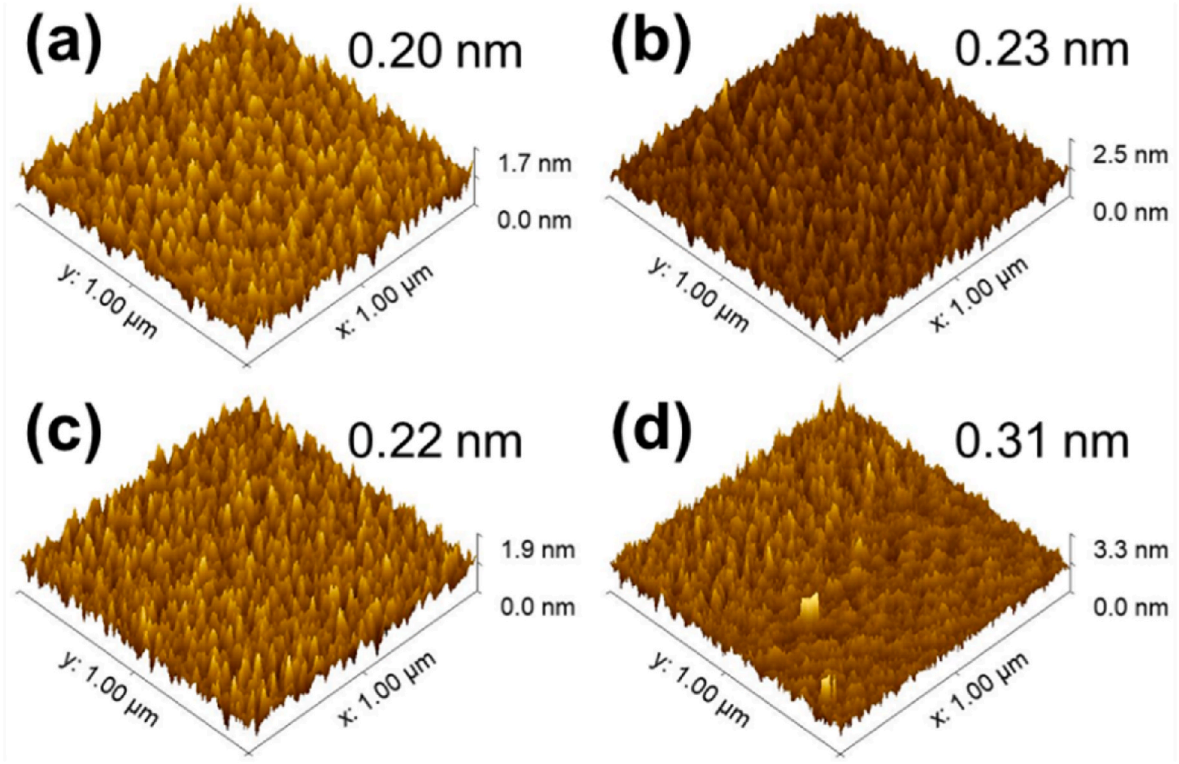

Fig. 7. AFM surface morphology of a-C:H films deposited at plasma powers of (a) 20, (b) 40, (c) 60, and (d) 80 W. The values in the top right corner of each image represent the RMS roughness value for each sample.

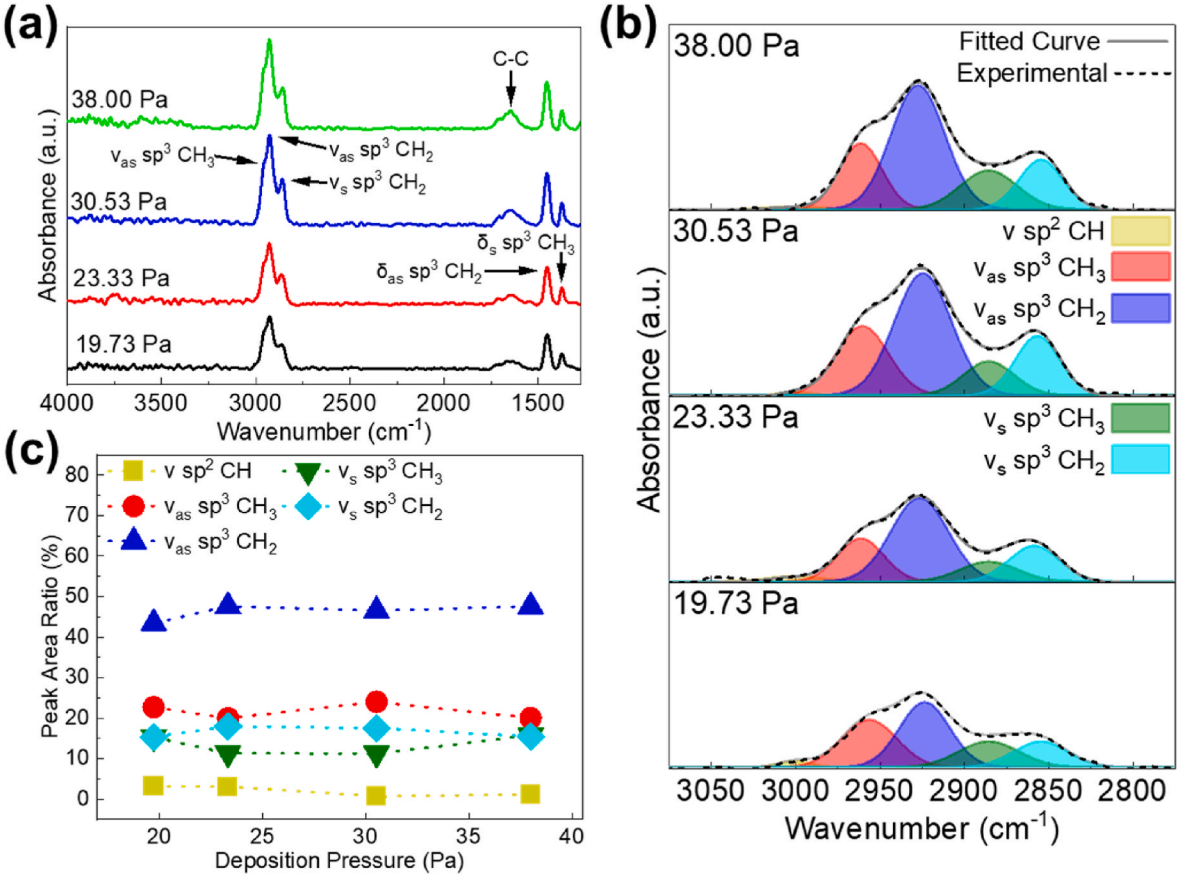

Fig. 8. (a) Stacked FTIR spectra, (b) deconvolution of CH_x, and (c) peak area ratio (PAR) of deconvoluted ν CH_x of a-C:H films deposited at varying deposition pressures between 19.73 and 37.80 Pa.

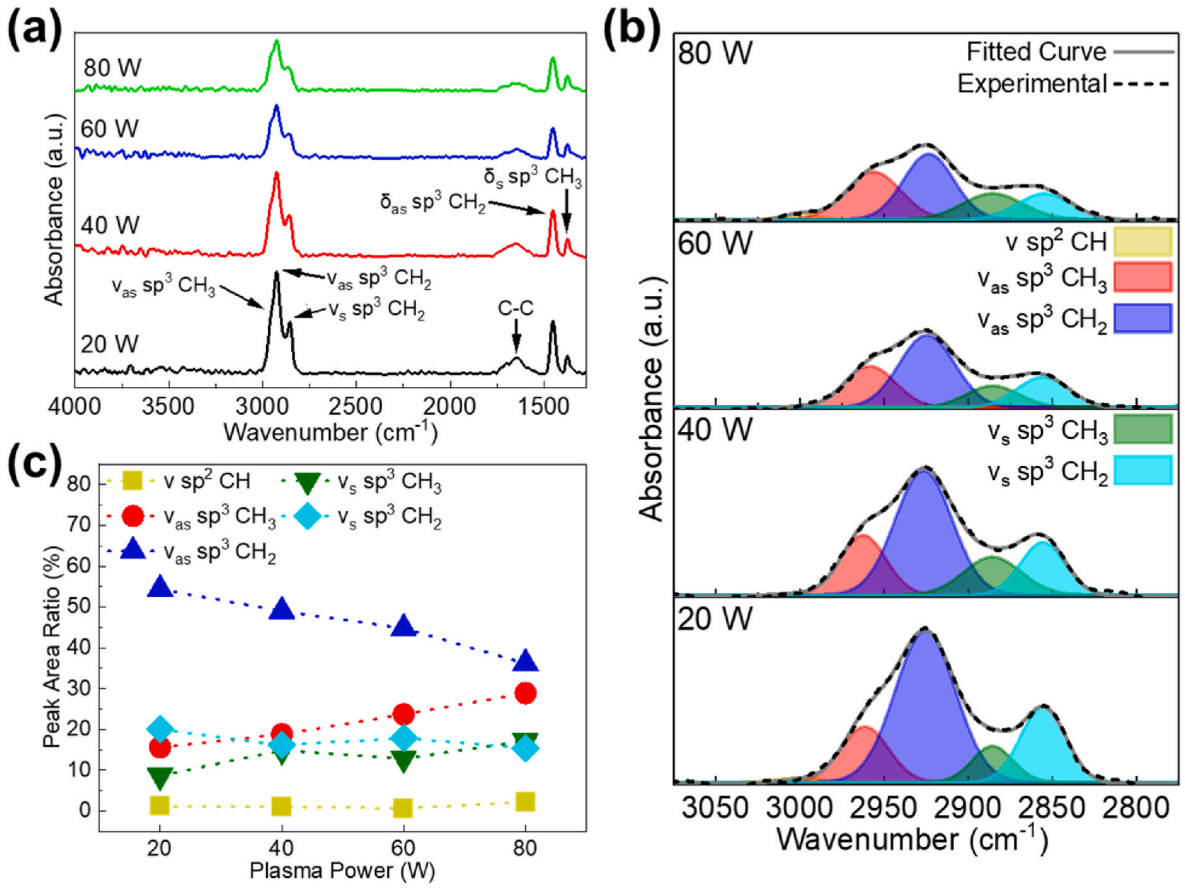

Fig. 9. (a) Stacked FTIR spectra, (b) deconvolution of CH_x, and (c) peak area ratio (PAR) of deconvoluted ν CH_x of a-C:H films deposited at varying plasma powers of 20, 40, 60, and 80 W.

the deposition pressure increased from 19.73 to 38.00 Pa, the RMS roughness decreased slightly from 0.31 to 0.27 nm.

Fig. 7(a)–(d) shows the surface morphology of the a-C:H films deposited at varying plasma powers. The RMS roughness value of the a-C:H films is displayed in the top right corner of each scan and in Table 2. As the plasma power increased from 20 to 80 W, the RMS roughness increased from 0.20 to 0.31 nm. The RMS roughness values of the a-C:H films for all deposition conditions were low compared to their film thickness (~40–100 nm), and the thinner samples tended to show decreased RMS roughness values compared to their thicker counterparts. It has been reported that increased roughness is indicative of increased porosity and hydrophobicity [39]. However, this trend is not consistent with what was found by this study. In fact, for the films deposited at varying pressures, hydrophobicity decreased as RMS roughness increased. No trend was observed between hydrophobicity and surface roughness for the films deposited at varying plasma powers.

3.3. FTIR analysis

An FTIR analysis was performed to determine the chemical composition of the a-C:H films deposited with varying deposition pressures and plasma powers. Fig. 8(a) shows the stacked FTIR spectra of the a-C:H films deposited at varying pressures between 19.73 and 38.00 Pa. There are several prominent features to be examined in the FTIR spectra. The two sharp peaks located at 1375 and 1450 cm^{-1} were associated with sp^3 CH_3 symmetric bending (δ_s sp^3 CH_3) and sp^3 CH_2 asymmetric bending (δ_{as} sp^3 CH_2), respectively [4]. The broad feature located from 1750 to 1500 cm^{-1} was caused by sp^2 C=C stretching (ν sp^2 C=C), and the large peak structure located from 3000 to 2800 cm^{-1} was caused by various CH_x stretching (ν CH_x) modes [4,9,13,37,40,41]. As the deposition pressure increased, the intensity of the ν CH_x peak prominently increased while the intensity of the δ_{as} sp^3 CH_2 peak increased slightly and the intensity of the δ_s sp^3 CH_3 peak remained consistent. It is apparent from the broadness of the ν sp^2 C=C peak that it is composed of several component peaks, confirming the amorphous nature of the films [39,42]. The intensity of the ν sp^2 C=C peak slightly increased as pressure increased. The presence of a large ν CH_x peak structure is consistent with what is found for other polymer-like a-C:H materials [16,21,24]. The intensity of the ν CH_x peak structure decreased significantly as pressure decreased, indicating a reduction in hydrogen content for a-C:H films formed by more energetic plasmas [27,39]. As the hydrogen content was reduced, an increased amount of sp^2 C-C bonding was able to form, consistent with the results seen in the refractive index analysis [26,36]. Fig. 8(b) shows the deconvolution of the ν CH_x peak structure into its five component peaks: sp^2 CH stretching (ν sp^2 CH), sp^3 CH_3 asymmetric stretching (ν_{as} sp^3 CH_3), sp^3 CH_2 asymmetric stretching (ν_{as} sp^3 CH_2), sp^3 CH_3 symmetric stretching (ν_s sp^3 CH_3), and sp^3 CH_2 symmetric stretching (ν_s sp^3 CH_2) located at their corresponding wavenumbers of 3035–3000, 2965–2955, 2930–2915, 2885–2870, 2875-2860 cm^{-1}, respectively [27,43]. The fraction of each component peak was different depending on the deposition pressures. The ν_{as} sp^3 CH_2 was dominant for all deposition pressures. Fig. 8(c) shows the peak area ratio (PAR) of the component peaks of the ν CH_x peak structure. It can be seen that sp^3 bonding accounts for most of the observed peak, and that only a small fraction can be assigned to sp^2 bonding. This is consistent with what is seen for other polymer-like a-C:H films [21]. The largest portion of the ν_{as} sp^3 CH_2 was observed with the PAR of 43.45–47.61 %, followed by ν_{as} sp^3 CH_3, ν_s sp^3 CH_2, and ν_s sp^3 CH_3 for all deposition pressures. A very small fraction below 3.18 % was observed for ν sp^2 CH.

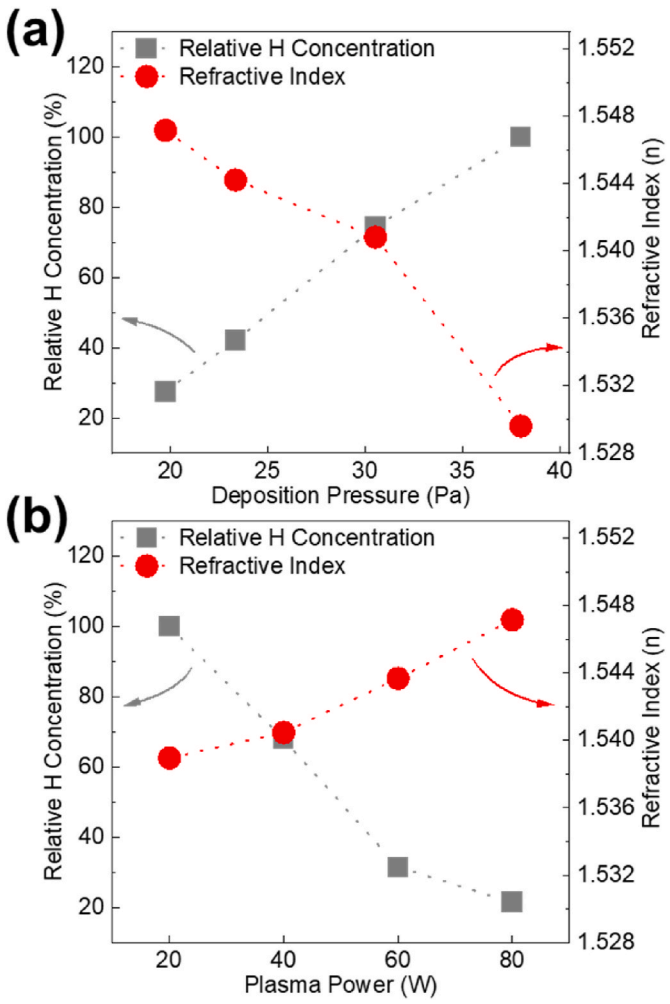

Fig. 10. Relative hydrogen concentration and refractive index of a-C:H films deposited with (a) varying deposition pressures between 19.73 and 38.00 Pa, and (b) varying plasma powers of 20, 40, 60, and 80 W.

Fig. 9(a) shows the stacked FTIR spectra of the a-C:H films deposited at varying plasma powers of 20, 40, 60, and 80 W. Similar features are seen in the FTIR spectra compared to the films deposited at varying pressures. As the plasma power increased, the intensity of the ν CH_x peak significantly decreased while the intensity of the δ_{as} sp^3 CH_2 peak decreased slightly and the intensity of the δ_s sp^3 CH_3 peak remained consistent. The increased intensity of the ν CH_x peak indicated a reduction in hydrogen content in the film. This along with the refractive index analysis supports the idea that a-C:H films formed by more energetic plasmas have a reduced concentration of hydrogen. The broadness of the ν sp^2 C=C peak confirms the amorphous nature of the films. The intensity of the ν sp^2 C=C peak slightly decreased as the plasma power increased. Fig. 9(b) shows the deconvolution of the ν CH_x peak structure into five component peaks of the ν sp^2 CH, ν_{as} sp^3 CH_3, ν_{as} sp^3 CH_2, ν_s sp^3 CH_3, and ν_s sp^3 CH_2 with varying plasma powers. As observed in the deconvolution at varying deposition pressures, the ν_{as} sp^3 CH_2 was dominant for all plasma powers. Fig. 9(c) shows the PAR of the five component peaks. As the plasma power increased from 20 to 80 W, the PAR of ν_{as} sp^3 CH_2 significantly decreased from 54.36 to 36.19 %. The PAR of the ν_{as} sp^3 CH_3 peak increased with increasing plasma power, from a minimum value of 15.64 % for the film deposited at 20 W to a maximum value of 28.91 % for the film deposited at 80 W. The PAR of the ν_s sp^3 CH_2 peak tended to decrease with increasing plasma power, with from a maximum value of 20.09 % for 20 W to a minimum value of 15.45 % for 80 W. The PAR of the ν_s sp^3 CH_3 peak tended to increase with increasing plasma power, from a minimum value of 8.65 % for 20 W to a maximum value of 17.20 % for 80 W. Similar to the a-C:H films deposited at varying pressures, the ν sp^2 CH peak was only present in small amounts below 2.25 %.

Fig. 10(a) and (b) presents the relative hydrogen concentration and refractive index of the a-C:H films deposited at varying deposition pressures and plasma powers, respectively. As stated in the experimental details section, the relative hydrogen content (C) was calculated by $C = A\int\frac{\alpha}{\omega}d\omega$, over the range of the ν CH_x peak structure at 3100-2800 cm^{-1}, where α is the absorption coefficient, ω is wavenumber in cm^{-1}, and A is a constant scaling factor [30–32]. It should be noted that unbound hydrogen is present within the a-C:H films, which is optically inactive and does not appear in the FTIR spectra [24,33]. As such, this method of estimating the relative hydrogen content assumes that the ratio between bound and unbound hydrogen is consistent between each sample. As the deposition pressure decreased from 38.00 to 19.73 Pa, the relative hydrogen content decreased from 100.00 to 27.48 %. Over this same change in the pressure, the refractive index increased from 1.530 to 1.547. As the plasma power increased from 20 to 80 W, the relative hydrogen content decreased from 100 to 21.51 %, while the refractive index increased from 1.539 to 1.547. The relative hydrogen content was reduced for the a-C:H films deposited at lower pressures and higher plasma powers, which is consistent with the idea that an increasingly energetic plasma removes more hydrogen from the film through additional ion bombardment during deposition [26]. As the amount of hydrogen within the film is reduced, additional sp^2 C-C sites form, promoting cross-linking and increasing the density of the films [26,36]. The increase in density is confirmed by the trend of refractive index to increase at lower pressures and higher plasma powers.

4. Summary and conclusions

Hydrogenated amorphous carbon (a-C:H) thin films were fabricated through PECVD of the cyclohexane precursor at varying deposition pressures and plasma powers. The films created were optically transparent, smooth, and hydrophobic. A wide optical bandgap range of 3.08–3.69 eV was obtained. The refractive index increased as the deposition pressure decreased and the plasma power increased, while relative hydrogen content decreased over the same change in parameters. The removal of hydrogen content promoted cross-linking between the remaining carbon atoms and improved the film density. The observed film characteristics could be advantageous for several potential applications including protective, wear-resistant, low-friction, or anti-reflective coatings for optical windows. Additional testing must be conducted to characterize the films' mechanical, tribological, and optical properties more fully before they can be tuned towards specific applications. The ability achieve high deposition rates at ambient temperature could also be advantageous for application on substrates with poor temperature resistance, such as polymers.

Ethical statement

Research results are not misrepresented. The results are presented clearly, honestly and without fabrication, falsification or inappropriate data manipulation. The results are appropriately placed in the context of prior and existing research. No data, text, or theories by others are presented as if they were the author's own.

This is the authors' own original work, which has not been previously published elsewhere. The manuscript is not currently being considered for publication elsewhere. The manuscript reflects the authors' own research and analysis in a truthful and complete manner.

The manuscript properly credits the meaningful contributions of co-authors. All authors have been personally and actively involved in substantial work leading to the manuscript and will take public responsibility for its content.

CRediT authorship contribution statement

Thomas Poche: Writing – original draft, Visualization, Validation, Methodology, Investigation, Formal analysis, Data curation. **Rajib Chowdhury:** Methodology, Investigation, Formal analysis, Data curation. **Seonhee Jang:** Writing – review & editing, Supervision, Resources, Project administration, Funding acquisition, Conceptualization.

Declaration of competing interest

The authors declare that they have no known competing financial interests or personal relationships that could have appeared to influence the work reported in this paper.

Data availability

Data will be made available on request.

Acknowledgements

This work was supported by the National Science Foundation under Grant No. CMMI 2026801. The authors would like to thank the Nanofabrication Facility at Louisiana State University for use of nanofabrication equipment.

References

[1] P.K. Chu, L. Li, Characterization of amorphous and nanocrystalline carbon films, Mater. Chem. Phys. 96 (2006) 253–277, https://doi.org/10.1016/j.matchemphys.2005.07.048.
[2] A.C. Ferrari, B. Kleinsorge, G. Adamopoulos, J. Robertson, W.I. Milne, V. Stolojan, L.M. Brown, A. LiBassi, B.K. Tanner, Determination of bonding in amorphous carbons by electron energy loss spectroscopy, Raman scattering and X-ray reflectivity, J. Non-Cryst. 266 (2000) 765–768, https://doi.org/10.1016/S0022-3093(00)00035-1.
[3] K.B.K. Teo, A.C. Ferrari, G. Fanchini, S.E. Rodil, J. Yuan, J.T.H. Tsai, E. Laurenti, A. Tagliaferro, J. Robertson, W.I. Milne, Highest optical gap tetrahedral amorphous carbon, Diam. Relat. Mater. 11 (2002) 1086–1090, https://doi.org/10.1016/S0925-9635(01)00591-X.
[4] V. Ţucureanu, A. Matei, A.M. Avram, FTIR spectroscopy for carbon family study, Crit. Rev. Anal. Chem. 46 (2016) 502–520, https://doi.org/10.1080/10408347.2016.1157013.
[5] J. Robertson, Diamond-like amorphous carbon, Mater. Sci. Eng. R Rep. 37 (2002) 129–281, https://doi.org/10.1016/S0927-796X(02)00005-0.
[6] B.-S. An, Y. Kwon, J.-S. Oh, C. Lee, S. Choi, H. Kim, M. Lee, S. Pae, C.-W. Yang, Characteristics of an amorphous carbon layer as a diffusion barrier for an advanced copper interconnect, ACS Appl. Mater. Interfaces 12 (2020) 3104–3113, https://doi.org/10.1021/acsami.9b15562.
[7] J. Kurokawa, H. Kondo, T. Tsutsumi, K. Ishikawa, M. Sekine, M. Hori, Effects of deposition precursors of hydrogenated amorphous carbon films on the plasma etching resistance based on mass spectrometer measurements and machine learning analysis, Vacuum 205 (2022) 111351, https://doi.org/10.1016/j.vacuum.2022.111351.
[8] J.J. Heikkinen, E. Peltola, N. Wester, J. Koskinen, T. Laurila, S. Franssila, V. Jokinen, Fabrication of micro- and nanopillars from pyrolytic carbon and tetrahedral amorphous carbon, Micromachines 10 (2019) 510, https://doi.org/10.3390/mi10080510.
[9] G. Adamopoulos, J. Robertson, N.A. Morrison, C. Godet, Hydrogen content estimation of hydrogenated amorphous carbon by visible Raman spectroscopy, J. Appl. Phys. 96 (2004) 6348–6352, https://doi.org/10.1063/1.1811397.
[10] B.S. Kwon, J.S. Kim, Ultrahigh selective etching of SiO_2 using an amorphous carbon mask in dual-frequency capacitively coupled $CF_8/CH_2F_2/O_2$/Ar plasmas, J. Electrochem. Soc. 157 (2010) D135–D141, https://doi.org/10.1149/1.3275710.
[11] D.K. Rajak, A. Kumar, A. Behera, P.L. Menezes, Diamond-like carbon (DLC) coatings: classification, properties, and applications, Appl. Sci. 11 (2021) 4445, https://doi.org/10.3390/app11104445.
[12] A.J. Bullen, K.E. O'Hara, D.G. Cahill, O. Monteiro, A. Von Keudell, Thermal conductivity of amorphous carbon thin films, J. Appl. Phys. 88 (2000) 6317–6320, https://doi.org/10.1063/1.1314301.
[13] J. Jaglarz, K. Dyndał, K. Tkacz-Śmiech, Thermo-optical properties of hydrogenated amorphous carbon and nitrogen-modified carbon layers from in situ ellipsometric studies, J. Mater. Res. Technol. 9 (2020) 1698–1707, https://doi.org/10.1016/j.jmrt.2019.11.093.
[14] J. Filik, P.W. May, S.R.J. Pearce, R.K. Wild, K.R. Hallam, XPS and laser Raman analysis of hydrogenated amorphous carbon films, Diam. Relat. Mater. 12 (2003) 974–978, https://doi.org/10.1016/S0925-9635(02)00374-6.
[15] A. Grill, Amorphous carbon based materials as the interconnect dielectric in ULSI chips, Diam. Relat. Mater. 10 (2001) 234–239, https://doi.org/10.1016/S0925-9635(00)00473-8.
[16] J.G. Buijnsters, R. Gago, I. Jiménez, M. Camero, F. Agulló-Rueda, C. Gómez-Aleixandre, Hydrogen quantification in hydrogenated amorphous carbon films by infrared, Raman, and x-ray absorption near edge spectroscopies, J. Appl. Phys. 105 (2009) 093510, https://doi.org/10.1063/1.3103326.
[17] V. Uskoković, A historical review of glassy carbon: synthesis, structure, properties and applications, Carbon Trends 5 (2021) 100116, https://doi.org/10.1016/j.cartre.2021.100116.
[18] Z. Zhai, H. Shen, J. Chen, X. Li, Y. Jiang, Evolution of structural and electrical properties of carbon films from amorphous carbon to nanocrystalline graphene on quartz glass by HFCVD, ACS Appl. Mater. Interfaces 10 (2018) 17427–17436, https://doi.org/10.1021/acsami.8b01588.
[19] Y. Lifshitz, Hydrogen-free amorphous carbon films: correlation between growth conditions and properties, Diam. Relat. Mater. 5 (1996) 388–400, https://doi.org/10.1016/0925-9635(95)00445-9.
[20] K. Endo, K. Shinoda, T. Tatsumi, Plasma deposition of low-dielectric-constant fluorinated amorphous carbon, J. Appl. Phys. 86 (1999) 2739–2745, https://doi.org/10.1063/1.371119.
[21] S.V. Singh, T. Zaharia, M. Creatore, R. Groenen, K. Van Hege, M.C.M. Van De Sanden, Hard graphitelike hydrogenated amorphous carbon grown at high rates by a remote plasma, J. Appl. Phys. 107 (2010) 013305, https://doi.org/10.1063/1.3273412.
[22] M. Tomidokoro, S. Tunmee, U. Rittihong, C. Euaruksakul, R. Supruangnet, H. Nakajima, Y. Hirata, N. Ohtake, H. Akasaka, Electrical conduction properties of hydrogenated amorphous carbon films with different structures, Materials 14 (2021) 2355, https://doi.org/10.3390/ma14092355.
[23] R.U.A. Khan, D. Grambole, S.R.P. Silva, Studies of carbon ion self-implantation into hydrogenated amorphous carbon films, Diam. Relat. Mater. 9 (2000) 675–679, https://doi.org/10.1016/S0925-9635(99)00340-4.
[24] J.W.A.M. Gielen, P.R.M. Kleuskens, M.C.M. Van De Sanden, L.J. Van Ijzendoorn, D. C. Schram, E.H.A. Dekempeneer, J. Meneve, Optical and mechanical properties of plasma-beam-deposited amorphous hydrogenated carbon, J. Appl. Phys. 80 (1996) 5986–5995, https://doi.org/10.1063/1.363567.
[25] E.A. Konshina, Amorphous hydrogenated carbon films with diamond-like and polymer-like properties, in: P. Mandracci (Ed.), Crystalline and Non-crystalline Solids, InTech, 2016, https://doi.org/10.5772/62704.
[26] A. Grill, Diamond-like carbon: state of the art, Diam. and Relat, Materials 8 (1999) 428–434, https://doi.org/10.1016/S0925-9635(98)00262-3.
[27] Young-Ho Son, Woo-Chul Jung, Jae-In Jeong, FTIR Characteristics of Hydrogenated Amorphous Carbon Films Prepared by ECR-PECVD, JKPS, vol. 39, 2001, pp. 713–717.
[28] N.A. Lange, Lange's Handbook of Chemistry, seventeenth ed., McGraw-Hill Education, New York, 2017.
[29] A.S. Ferlauto, G.M. Ferreira, J.M. Pearce, C.R. Wronski, R.W. Collins, X. Deng, G. Ganguly, Analytical model for the optical functions of amorphous semiconductors and its applications for thin film solar cells, Thin Solid Films 455–456 (2004) 388–392, https://doi.org/10.1016/j.tsf.2003.11.234.
[30] S. Alotaibi, K. Nama Manjunatha, S. Paul, Stability of hydrogenated amorphous carbon thin films for application in electronic devices, Diam. Relat. Mater. 90 (2018) 172–180, https://doi.org/10.1016/j.diamond.2018.10.016.
[31] S. Paul, Growth, Characterisation and Electronic Applications of Amorphous Hydrogenated Carbon, 2000.
[32] S. Liu, S. Gangopadhyay, G. Sreenivas, S.S. Ang, H.A. Naseem, Infrared studies of hydrogenated amorphous carbon (a-C:H) and its alloys (a-C:H,N,F), Phys. Rev. B 55 (1997) 13020–13024, https://doi.org/10.1103/PhysRevB.55.13020.
[33] A. Grill, V. Pate, Characterization of diamondike carbon by infrared spectroscopy? Appl. Phys. Lett. 60 (1992) 2089–2091, https://doi.org/10.1063/1.107098.
[34] W. Wirth, J. Comeaux, S. Jang, Characterization of flexible low-dielectric constant carbon-doped oxide (SiCOH) thin films under repeated mechanical bending stress, J. Mater. Sci. 57 (2022) 21411–21431, https://doi.org/10.1007/s10853-022-07987-y.
[35] A.C. Ferrari, A. Libassi, B.K. Tanner, V. Stolojan, J. Yuan, L.M. Brown, S.E. Rodil, B. Kleinsorge, J. Robertson, Density, sp^3 fraction, and cross-sectional structure of amorphous carbon films determined by x-ray reflectivity and electron energy-loss spectroscopy, Phys. Rev. B 62 (2000) 11089–11103, https://doi.org/10.1103/PhysRevB.62.11089.
[36] S. Pisana, S.K. O'Leary, S. Zukotynski, Optical properties of hydrogenated amorphous carbon thin films prepared by dc saddle field plasma-enhanced chemical vapor deposition, J. Non-Cryst. 351 (2005) 736–740, https://doi.org/10.1016/j.jnoncrysol.2005.01.056.
[37] Y. Taki, O. Takai, XPS structural characterization of hydrogenated amorphous carbon thin films prepared by shielded arc ion plating, Thin Solid Films 316 (1998) 45–50, https://doi.org/10.1016/S0040-6090(98)00386-1.
[38] D. Padhi, B.H. Kim, D. Witty, Dry etch selectivity of a-C:H hardmasks for sub-65nm patterning applications, J. Vac. Sci. Technol., B: Nanotechnol. Microelectron. 27 (2009) 1809–1812, https://doi.org/10.1116/1.3151836.
[39] D. Banerjee, S. Mukherjee, K.K. Chattopadhyay, Controlling the surface topology and hence the hydrophobicity of amorphous carbon thin films, Carbon 48 (2010) 1025–1031, https://doi.org/10.1016/j.carbon.2009.11.021.
[40] K. Gao, Y. Wang, X. Wei, L. Qiang, B. Zhang, J. Zhang, Hydrogenated amorphous carbon films with different nanostructure: a comparative study, Chem. Phys. Lett. 715 (2019) 330–334, https://doi.org/10.1016/j.cplett.2018.11.028.

[41] J.M. Jaramillo, R.D. Mansano, L.S. Zambom, M. Massi, H.S. Maciel, Wet etching of hydrogenated amorphous carbon films, Diam. Relat. Mater. 10 (2001) 976–979, https://doi.org/10.1016/S0925-9635(00)00584-7.
[42] A.M. De Oliveira Neto, W.H. Schreiner, J.F. Justo, A.M. De Oliveira, E.C. Rangel, S. F. Durrant, Characterization of amorphous carbon films by PECVD and plasma ion implantation: the role of fluorine and sulfur doping, Mater. Chem. Phys. 227 (2019) 170–175, https://doi.org/10.1016/j.matchemphys.2019.02.008.
[43] J.V. Anguita, S.R.P. Silva, A.P. Burden, B.J. Sealy, S. Haq, M. Hebbron, I. Sturland, A. Pritchard, Thermal stability of plasma deposited thin films of hydrogenated carbon–nitrogen alloys, J. Appl. Phys. 86 (1999) 6276–6281, https://doi.org/10.1063/1.371685.